Measurement of the Branching Fractions of the Color-Suppressed Decays $\overline{B}^0 \to D^0\pi^0$, $D^{*0}\pi^0$, $D^0\eta$, $D^{*0}\eta$, $D^0\omega$, $D^{*0}\omega$, $D^0\eta'$, and $D^{*0}\eta'$

The BABAR Collaboration

August 5, 2008

We report results on the branching fraction ($\mathcal{BF}$) measurement of the color-suppressed decays $\overline{B}^0 \to D^0\pi^0$, $D^{*0}\pi^0$, $D^0\eta$, $D^{*0}\eta$, $D^0\omega$, $D^{*0}\omega$, $D^0\eta'$, and $D^{*0}\eta'$. We measure the branching fractions $\mathcal{BF}(D^0\pi^0) = (2.78 \pm 0.08 \pm 0.20) \times 10^{-4}$, $\mathcal{BF}(D^{*0}\pi^0) = (1.78 \pm 0.13 \pm 0.23) \times 10^{-4}$, $\mathcal{BF}(D^0\eta) = (2.41 \pm 0.09 \pm 0.17) \times 10^{-4}$, $\mathcal{BF}(D^{*0}\eta) = (2.32 \pm 0.13 \pm 0.22) \times 10^{-4}$, $\mathcal{BF}(D^0\omega) = (2.77 \pm 0.13 \pm 0.22) \times 10^{-4}$, $\mathcal{BF}(D^{*0}\omega) = (4.44 \pm 0.23 \pm 0.61) \times 10^{-4}$, $\mathcal{BF}(D^0\eta') = (1.38 \pm 0.12 \pm 0.22) \times 10^{-4}$ and $\mathcal{BF}(D^{*0}\eta') = (1.29 \pm 0.23 \pm 0.23) \times 10^{-4}$, where the first uncertainty is statistical and the second is systematic. The result is based on a sample of $(454 \pm 5) \times 10^6 B\overline{B}$ pairs collected at the $\Upsilon(4S)$ resonance from 1999 to 2007, with the BABAR detector at the PEP-II storage rings at the Stanford Linear Accelerator Center. The measurements are compared to theoretical predictions by factorization, SCET and pQCD. The presence of final state interactions is confirmed and the measurements seem to be more in favor of SCET compared to pQCD.

The BABAR Collaboration,

B. Aubert, M. Bona, Y. Karyotakis, J. P. Lees, V. Poireau, E. Prencipe, X. Prudent, V. Tisserand

Laboratoire de Physique des Particules, IN2P3/CNRS et Université de Savoie, F-74941 Annecy-Le-Vieux, France

J. Garra Tico, E. Grauges

Universitat de Barcelona, Facultat de Fisica, Departament ECM, E-08028 Barcelona, Spain

L. Lopez[ab], A. Palano[ab], M. Pappagallo[ab]

INFN Sezione di Bari[a]; Dipartmento di Fisica, Università di Bari[b], I-70126 Bari, Italy

G. Eigen, B. Stugu, L. Sun

University of Bergen, Institute of Physics, N-5007 Bergen, Norway

G. S. Abrams, M. Battaglia, D. N. Brown, R. N. Cahn, R. G. Jacobsen, L. T. Kerth, Yu. G. Kolomensky, G. Lynch, I. L. Osipenkov, M. T. Ronan,[1] K. Tackmann, T. Tanabe

Lawrence Berkeley National Laboratory and University of California, Berkeley, California 94720, USA

C. M. Hawkes, N. Soni, A. T. Watson

University of Birmingham, Birmingham, B15 2TT, United Kingdom

H. Koch, T. Schroeder

Ruhr Universität Bochum, Institut für Experimentalphysik 1, D-44780 Bochum, Germany

D. Walker

University of Bristol, Bristol BS8 1TL, United Kingdom

D. J. Asgeirsson, B. G. Fulsom, C. Hearty, T. S. Mattison, J. A. McKenna

University of British Columbia, Vancouver, British Columbia, Canada V6T 1Z1

M. Barrett, A. Khan

Brunel University, Uxbridge, Middlesex UB8 3PH, United Kingdom

V. E. Blinov, A. D. Bukin, A. R. Buzykaev, V. P. Druzhinin, V. B. Golubev, A. P. Onuchin, S. I. Serednyakov, Yu. I. Skovpen, E. P. Solodov, K. Yu. Todyshev

Budker Institute of Nuclear Physics, Novosibirsk 630090, Russia

M. Bondioli, S. Curry, I. Eschrich, D. Kirkby, A. J. Lankford, P. Lund, M. Mandelkern, E. C. Martin, D. P. Stoker

University of California at Irvine, Irvine, California 92697, USA

S. Abachi, C. Buchanan

University of California at Los Angeles, Los Angeles, California 90024, USA

J. W. Gary, F. Liu, O. Long, B. C. Shen,[1] G. M. Vitug, Z. Yasin, L. Zhang

University of California at Riverside, Riverside, California 92521, USA

---

[1]Deceased

2

V. Sharma

University of California at San Diego, La Jolla, California 92093, USA

C. Campagnari, T. M. Hong, D. Kovalskyi, M. A. Mazur, J. D. Richman

University of California at Santa Barbara, Santa Barbara, California 93106, USA

T. W. Beck, A. M. Eisner, C. J. Flacco, C. A. Heusch, J. Kroseberg, W. S. Lockman, A. J. Martinez,
T. Schalk, B. A. Schumm, A. Seiden, M. G. Wilson, L. O. Winstrom

University of California at Santa Cruz, Institute for Particle Physics, Santa Cruz, California 95064, USA

C. H. Cheng, D. A. Doll, B. Echenard, F. Fang, D. G. Hitlin, I. Narsky, T. Piatenko, F. C. Porter

California Institute of Technology, Pasadena, California 91125, USA

R. Andreassen, G. Mancinelli, B. T. Meadows, K. Mishra, M. D. Sokoloff

University of Cincinnati, Cincinnati, Ohio 45221, USA

P. C. Bloom, W. T. Ford, A. Gaz, J. F. Hirschauer, M. Nagel, U. Nauenberg, J. G. Smith, K. A. Ulmer,
S. R. Wagner

University of Colorado, Boulder, Colorado 80309, USA

R. Ayad,[2] A. Soffer,[3] W. H. Toki, R. J. Wilson

Colorado State University, Fort Collins, Colorado 80523, USA

D. D. Altenburg, E. Feltresi, A. Hauke, H. Jasper, M. Karbach, J. Merkel, A. Petzold, B. Spaan, K. Wacker

Technische Universität Dortmund, Fakultät Physik, D-44221 Dortmund, Germany

M. J. Kobel, W. F. Mader, R. Nogowski, K. R. Schubert, R. Schwierz, A. Volk

Technische Universität Dresden, Institut für Kern- und Teilchenphysik, D-01062 Dresden, Germany

D. Bernard, G. R. Bonneaud, E. Latour, M. Verderi

Laboratoire Leprince-Ringuet, CNRS/IN2P3, Ecole Polytechnique, F-91128 Palaiseau, France

P. J. Clark, S. Playfer, J. E. Watson

University of Edinburgh, Edinburgh EH9 3JZ, United Kingdom

M. Andreotti[ab], D. Bettoni[a], C. Bozzi[a], R. Calabrese[ab], A. Cecchi[ab], G. Cibinetto[ab], P. Franchini[ab],
E. Luppi[ab], M. Negrini[ab], A. Petrella[ab], L. Piemontese[a], V. Santoro[ab]

INFN Sezione di Ferrara[a]; Dipartimento di Fisica, Università di Ferrara[b], I-44100 Ferrara, Italy

R. Baldini-Ferroli, A. Calcaterra, R. de Sangro, G. Finocchiaro, S. Pacetti, P. Patteri, I. M. Peruzzi,[4]
M. Piccolo, M. Rama, A. Zallo

INFN Laboratori Nazionali di Frascati, I-00044 Frascati, Italy

A. Buzzo[a], R. Contri[ab], M. Lo Vetere[ab], M. M. Macri[a], M. R. Monge[ab], S. Passaggio[a], C. Patrignani[ab],
E. Robutti[a], A. Santroni[ab], S. Tosi[ab]

INFN Sezione di Genova[a]; Dipartimento di Fisica, Università di Genova[b], I-16146 Genova, Italy

[2]Now at Temple University, Philadelphia, Pennsylvania 19122, USA
[3]Now at Tel Aviv University, Tel Aviv, 69978, Israel
[4]Also with Università di Perugia, Dipartimento di Fisica, Perugia, Italy

3

K. S. Chaisanguanthum, M. Morii

Harvard University, Cambridge, Massachusetts 02138, USA

A. Adametz, J. Marks, S. Schenk, U. Uwer

Universität Heidelberg, Physikalisches Institut, Philosophenweg 12, D-69120 Heidelberg, Germany

V. Klose, H. M. Lacker

Humboldt-Universität zu Berlin, Institut für Physik, Newtonstr. 15, D-12489 Berlin, Germany

D. J. Bard, P. D. Dauncey, J. A. Nash, M. Tibbetts

Imperial College London, London, SW7 2AZ, United Kingdom

P. K. Behera, X. Chai, M. J. Charles, U. Mallik

University of Iowa, Iowa City, Iowa 52242, USA

J. Cochran, H. B. Crawley, L. Dong, W. T. Meyer, S. Prell, E. I. Rosenberg, A. E. Rubin

Iowa State University, Ames, Iowa 50011-3160, USA

Y. Y. Gao, A. V. Gritsan, Z. J. Guo, C. K. Lae

Johns Hopkins University, Baltimore, Maryland 21218, USA

N. Arnaud, J. Béquilleux, A. D'Orazio, M. Davier, J. Firmino da Costa, G. Grosdidier, A. Höcker,
V. Lepeltier, F. Le Diberder, A. M. Lutz, S. Pruvot, P. Roudeau, M. H. Schune, J. Serrano, V. Sordini,[5]
A. Stocchi, G. Wormser

Laboratoire de l'Accélérateur Linéaire, IN2P3/CNRS et Université Paris-Sud 11, Centre Scientifique d'Orsay, B. P. 34, F-91898 Orsay Cedex, France

D. J. Lange, D. M. Wright

Lawrence Livermore National Laboratory, Livermore, California 94550, USA

I. Bingham, J. P. Burke, C. A. Chavez, J. R. Fry, E. Gabathuler, R. Gamet, D. E. Hutchcroft, D. J. Payne,
C. Touramanis

University of Liverpool, Liverpool L69 7ZE, United Kingdom

A. J. Bevan, C. K. Clarke, K. A. George, F. Di Lodovico, R. Sacco, M. Sigamani

Queen Mary, University of London, London, E1 4NS, United Kingdom

G. Cowan, H. U. Flaecher, D. A. Hopkins, S. Paramesvaran, F. Salvatore, A. C. Wren

University of London, Royal Holloway and Bedford New College, Egham, Surrey TW20 0EX, United Kingdom

D. N. Brown, C. L. Davis

University of Louisville, Louisville, Kentucky 40292, USA

A. G. Denig M. Fritsch, W. Gradl, G. Schott

Johannes Gutenberg-Universität Mainz, Institut für Kernphysik, D-55099 Mainz, Germany

---

[5]Also with Università di Roma La Sapienza, I-00185 Roma, Italy

K. E. Alwyn, D. Bailey, R. J. Barlow, Y. M. Chia, C. L. Edgar, G. Jackson, G. D. Lafferty, T. J. West, J. I. Yi

University of Manchester, Manchester M13 9PL, United Kingdom

J. Anderson, C. Chen, A. Jawahery, D. A. Roberts, G. Simi, J. M. Tuggle

University of Maryland, College Park, Maryland 20742, USA

C. Dallapiccola, X. Li, E. Salvati, S. Saremi

University of Massachusetts, Amherst, Massachusetts 01003, USA

R. Cowan, D. Dujmic, P. H. Fisher, G. Sciolla, M. Spitznagel, F. Taylor, R. K. Yamamoto, M. Zhao

Massachusetts Institute of Technology, Laboratory for Nuclear Science, Cambridge, Massachusetts 02139, USA

P. M. Patel, S. H. Robertson

McGill University, Montréal, Québec, Canada H3A 2T8

A. Lazzaro[ab], V. Lombardo[a], F. Palombo[ab]

INFN Sezione di Milano[a]; Dipartimento di Fisica, Università di Milano[b], I-20133 Milano, Italy

J. M. Bauer, L. Cremaldi R. Godang,[6] R. Kroeger, D. A. Sanders, D. J. Summers, H. W. Zhao

University of Mississippi, University, Mississippi 38677, USA

M. Simard, P. Taras, F. B. Viaud

Université de Montréal, Physique des Particules, Montréal, Québec, Canada H3C 3J7

H. Nicholson

Mount Holyoke College, South Hadley, Massachusetts 01075, USA

G. De Nardo[ab], L. Lista[a], D. Monorchio[ab], G. Onorato[ab], C. Sciacca[ab]

INFN Sezione di Napoli[a]; Dipartimento di Scienze Fisiche, Università di Napoli Federico II[b], I-80126 Napoli, Italy

G. Raven, H. L. Snoek

NIKHEF, National Institute for Nuclear Physics and High Energy Physics, NL-1009 DB Amsterdam, The Netherlands

C. P. Jessop, K. J. Knoepfel, J. M. LoSecco, W. F. Wang

University of Notre Dame, Notre Dame, Indiana 46556, USA

G. Benelli, L. A. Corwin, K. Honscheid, H. Kagan, R. Kass, J. P. Morris, A. M. Rahimi, J. J. Regensburger, S. J. Sekula, Q. K. Wong

Ohio State University, Columbus, Ohio 43210, USA

N. L. Blount, J. Brau, R. Frey, O. Igonkina, J. A. Kolb, M. Lu, R. Rahmat, N. B. Sinev, D. Strom, J. Strube, E. Torrence

University of Oregon, Eugene, Oregon 97403, USA

---

[6]Now at University of South Alabama, Mobile, Alabama 36688, USA

5

G. Castelli^{ab}, N. Gagliardi^{ab}, M. Margoni^{ab}, M. Morandin^a, M. Posocco^a, M. Rotondo^a, F. Simonetto^{ab}, R. Stroili^{ab}, C. Voci^{ab}

INFN Sezione di Padova^a; Dipartimento di Fisica, Università di Padova^b, I-35131 Padova, Italy

P. del Amo Sanchez, E. Ben-Haim, H. Briand, G. Calderini, J. Chauveau, P. David, L. Del Buono, O. Hamon, Ph. Leruste, J. Ocariz, A. Perez, J. Prendki, S. Sitt

Laboratoire de Physique Nucléaire et de Hautes Energies, IN2P3/CNRS, Université Pierre et Marie Curie-Paris6, Université Denis Diderot-Paris7, F-75252 Paris, France

L. Gladney

University of Pennsylvania, Philadelphia, Pennsylvania 19104, USA

M. Biasini^{ab}, R. Covarelli^{ab}, E. Manoni^{ab},

INFN Sezione di Perugia^a; Dipartimento di Fisica, Università di Perugia^b, I-06100 Perugia, Italy

C. Angelini^{ab}, G. Batignani^{ab}, S. Bettarini^{ab}, M. Carpinelli^{ab},[7] A. Cervelli^{ab}, F. Forti^{ab}, M. A. Giorgi^{ab}, A. Lusiani^{ac}, G. Marchiori^{ab}, M. Morganti^{ab}, N. Neri^{ab}, E. Paoloni^{ab}, G. Rizzo^{ab}, J. J. Walsh^a

INFN Sezione di Pisa^a; Dipartimento di Fisica, Università di Pisa^b; Scuola Normale Superiore di Pisa^c, I-56127 Pisa, Italy

D. Lopes Pegna, C. Lu, J. Olsen, A. J. S. Smith, A. V. Telnov

Princeton University, Princeton, New Jersey 08544, USA

F. Anulli^a, E. Baracchini^{ab}, G. Cavoto^a, D. del Re^{ab}, E. Di Marco^{ab}, R. Faccini^{ab}, F. Ferrarotto^a, F. Ferroni^{ab}, M. Gaspero^{ab}, P. D. Jackson^a, L. Li Gioi^a, M. A. Mazzoni^a, S. Morganti^a, G. Piredda^a, F. Polci^{ab}, F. Renga^{ab}, C. Voena^a

INFN Sezione di Roma^a; Dipartimento di Fisica, Università di Roma La Sapienza^b, I-00185 Roma, Italy

M. Ebert, T. Hartmann, H. Schröder, R. Waldi

Universität Rostock, D-18051 Rostock, Germany

T. Adye, B. Franek, E. O. Olaiya, F. F. Wilson

Rutherford Appleton Laboratory, Chilton, Didcot, Oxon, OX11 0QX, United Kingdom

S. Emery, M. Escalier, L. Esteve, S. F. Ganzhur, G. Hamel de Monchenault, W. Kozanecki, G. Vasseur, Ch. Yèche, M. Zito

CEA, Irfu, SPP, Centre de Saclay, F-91191 Gif-sur-Yvette, France

X. R. Chen, H. Liu, W. Park, M. V. Purohit, R. M. White, J. R. Wilson

University of South Carolina, Columbia, South Carolina 29208, USA

M. T. Allen, D. Aston, R. Bartoldus, P. Bechtle, J. F. Benitez, R. Cenci, J. P. Coleman, M. R. Convery, J. C. Dingfelder, J. Dorfan, G. P. Dubois-Felsmann, W. Dunwoodie, R. C. Field, A. M. Gabareen, S. J. Gowdy, M. T. Graham, P. Grenier, C. Hast, W. R. Innes, J. Kaminski, M. H. Kelsey, H. Kim, P. Kim, M. L. Kocian, D. W. G. S. Leith, S. Li, B. Lindquist, S. Luitz, V. Luth, H. L. Lynch, D. B. MacFarlane, H. Marsiske, R. Messner, D. R. Muller, H. Neal, S. Nelson, C. P. O'Grady, I. Ofte, A. Perazzo, M. Perl, B. N. Ratcliff, A. Roodman, A. A. Salnikov, R. H. Schindler, J. Schwiening, A. Snyder, D. Su, M. K. Sullivan, K. Suzuki, S. K. Swain, J. M. Thompson, J. Va'vra, A. P. Wagner, M. Weaver, C. A. West, W. J. Wisniewski, M. Wittgen, D. H. Wright, H. W. Wulsin, A. K. Yarritu, K. Yi, C. C. Young, V. Ziegler

Stanford Linear Accelerator Center, Stanford, California 94309, USA

---

[7]Also with Università di Sassari, Sassari, Italy

P. R. Burchat, A. J. Edwards, S. A. Majewski, T. S. Miyashita, B. A. Petersen, L. Wilden

Stanford University, Stanford, California 94305-4060, USA

S. Ahmed, M. S. Alam, J. A. Ernst, B. Pan, M. A. Saeed, S. B. Zain

State University of New York, Albany, New York 12222, USA

S. M. Spanier, B. J. Wogsland

University of Tennessee, Knoxville, Tennessee 37996, USA

R. Eckmann, J. L. Ritchie, A. M. Ruland, C. J. Schilling, R. F. Schwitters

University of Texas at Austin, Austin, Texas 78712, USA

B. W. Drummond, J. M. Izen, X. C. Lou

University of Texas at Dallas, Richardson, Texas 75083, USA

F. Bianchi[ab], D. Gamba[ab], M. Pelliccioni[ab]

INFN Sezione di Torino[a]; Dipartimento di Fisica Sperimentale, Università di Torino[b], I-10125 Torino, Italy

M. Bomben[ab], L. Bosisio[ab], C. Cartaro[ab], G. Della Ricca[ab], L. Lanceri[ab], L. Vitale[ab]

INFN Sezione di Trieste[a]; Dipartimento di Fisica, Università di Trieste[b], I-34127 Trieste, Italy

V. Azzolini, N. Lopez-March, F. Martinez-Vidal, D. A. Milanes, A. Oyanguren

IFIC, Universitat de Valencia-CSIC, E-46071 Valencia, Spain

J. Albert, Sw. Banerjee, B. Bhuyan, H. H. F. Choi, K. Hamano, R. Kowalewski, M. J. Lewczuk, I. M. Nugent, J. M. Roney, R. J. Sobie

University of Victoria, Victoria, British Columbia, Canada V8W 3P6

T. J. Gershon, P. F. Harrison, J. Ilic, T. E. Latham, G. B. Mohanty

Department of Physics, University of Warwick, Coventry CV4 7AL, United Kingdom

H. R. Band, X. Chen, S. Dasu, K. T. Flood, Y. Pan, M. Pierini, R. Prepost, C. O. Vuosalo, S. L. Wu

University of Wisconsin, Madison, Wisconsin 53706, USA

1 INTRODUCTION

Weak decays of hadrons provide a straight access to the parameters of the CKM matrix and thus to the study of the *CP* violation. Gluon scattering in the final state (Final State Interactions, or FSI) can modify the decay dynamics and so must be well understood. The two-body hadronic decays with a charmed final state, $B \to Dh$, are of great help in studying strong-interaction physics related with the confinement of quarks and gluons into hadrons.

The decays $B \to Dh$, where h is a light meson, can proceed through the emission of a $W^\pm$ boson following three possible diagrams: external, internal (see Fig. 1) or by a $W^\pm$ boson exchange whose contribution is negligible [1].
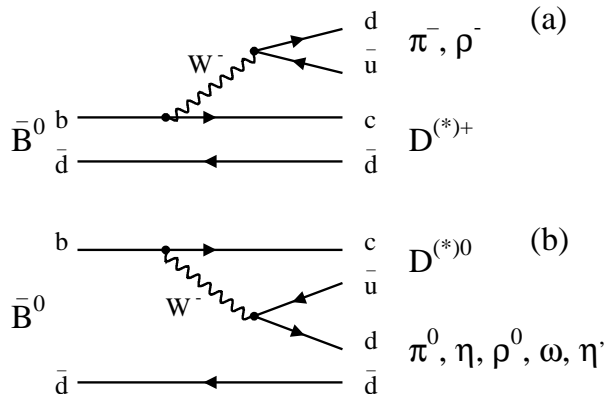

Figure 1: External (a) and internal (b) tree diagrams for $\overline{B}^0 \to Dh$ decays.

In the case of the decays $\overline{B}^0 \to D^{(*)0}h^0$, the major contribution comes from the internal diagram [2]. Since mesons are color single objects, in internal diagrams $\overline{B}^0 \to D^{(*)0}h^0$ the quarks from the $W^\pm$ decay are constrained to have the anti-color of the spectator quark, which induces a suppression of internal diagrams in comparison with external ones. Internal diagrams are so called *color-suppressed* and external ones are called *color-favored*.

In the factorization model [2, 3, 4, 5], the non-factorizable interactions in the final state by soft gluons are neglected. The matrix element in the effective weak Hamiltonian of the decay $B \to Dh$ is then factorized into a product of asymptotic states. Factorization appears to be successful in the description of the color-favored decays [6].

The decays $\overline{B}^0 \to D^{(*)0}\pi^0$ were first observed by CLEO [7] and Belle [8] with respectively 9.67 and 23.1×10^6 $B\overline{B}$ pairs. The Belle collaboration has also observed the decays $D^0\eta$ and $D^0\omega$ and put upper limits on the $\mathcal{BF}$ of $D^{*0}\eta$ and $D^{*0}\omega$ [8].

The branching fraction ($\mathcal{BF}$) of the color-suppressed decays $\overline{B}^0 \to D^{(*)0}\pi^0$, $D^{(*)0}\eta$, $D^{(*)0}\omega$, and $D^0\eta'$ were measured recently by *BABAR* [9] with 88×10^6 $B\overline{B}$ pairs and an upper limit was set on the $\mathcal{BF}$ of $D^{*0}\eta'$. The Belle collaboration measured with 152×10^6 $B\overline{B}$ pairs the $\mathcal{BF}$ of $\overline{B}^0 \to D^{(*)0}h^0$, $h^0 = \pi^0$, η, ω, and η' [10, 11] and studied the decays $\overline{B}^0 \to D^{(*)0}\rho^0$ with 388×10^6 $B\overline{B}$ pairs [12]. Many of these measurements showed a significant disagreement with predictions by factorization [13], but stronger experimental constraints are needed to distinguish between the different models of the color-suppressed dynamics like pQCD (*perturbative QCD*) [14, 15] or SCET (*Soft Collinear Effective Theory*) [16, 17, 18]. This paper reports the branching fraction measurement of eight color-suppressed decays $\overline{B}^0 \to D^{(*)0}\pi^0$, $D^{(*)0}\eta$, $D^{(*)0}\omega$ and $D^{(*)0}\eta'$ with 454×10^6 $B\overline{B}$ pairs.

2   THE *BABAR* DETECTOR AND DATASET

The data used in this analysis were collected with the *BABAR* detector at the PEP-II asymmetric e^+e^- storage ring. The *BABAR* detector is described in detail in Ref. [19]. Charged particle tracks are reconstructed using a five-layer silicon vertex tracker (SVT) and a 40-layer drift chamber (DCH) immersed in a 1.5 T magnetic field. Tracks are identified as pions or kaons (particle identification or PID) based on likelihoods constructed from energy loss measurements in the SVT and the DCH and from Cherenkov radiation angles measured in the detector of Cherenkov light (DIRC). Photons are reconstructed from showers measured in the electromagnetic calorimeter (EMC). Muon and neutral hadron identification are performed with the instrumented flux return (IFR).

The data sample consists of an integrated luminosity of 413 fb^{-1} recorded at the $\Upsilon(4S)$ resonance with a center-of-mass (CM) energy of 10.58 GeV, corresponding to $(454 \pm 5) \times 10^6$ $B\overline{B}$ pairs. A data sample of 41 fb^{-1} with a CM energy 40 MeV below the $\Upsilon(4S)$ resonance is used to study background contributions from continuum events $e^+e^- \rightarrow q\overline{q}$ ($q = u,\ d,\ s,\ c$).

Samples of simulated Monte Carlo (MC) events were used to determine signal and background characteristics, optimize selection criteria and evaluate efficiencies. Simulated events $e^+e^- \rightarrow \Upsilon(4S) \rightarrow B^+B^-$, $B^0\overline{B}^0$, $e^+e^- \rightarrow q\overline{q}$ ($q = u,\ d,\ s$) and $e^+e^- \rightarrow c\overline{c}$ are generated with `EvtGen` [20], which interfaces to `Pythia` [21] and `Jetset` [22]. Separate samples of exclusive $\overline{B}^0 \rightarrow D^{(*)0}h^0$ decays were generated to evaluate the signal features and the efficiency of selections on signal. A sample of exclusive $B^- \rightarrow D^{(*)0}\rho^-$ was generated for the study of that background. All MC samples include simulation of the *BABAR* detector response generated through `GEANT4` [23]. The integrated luminosity of the MC samples is about three times the data luminosity for $B\overline{B}$, one times the data luminosity for $e^+e^- \rightarrow q\overline{q}$ ($q = u,\ d,\ s$) and two times for $e^+e^- \rightarrow c\overline{c}$. The equivalent integrated luminosities of the exclusive simulations range from 50 to 2500 times the data luminosity.

3   ANALYSIS METHOD

3.1   Event reconstruction

Charged particles tracks are reconstructed from measurements in the SVT and/or the DCH, and an identification is assigned by the PID algorithm. Extrapolated tracks must be in the vicinity of the e^+e^- interaction point, *i.e.* within 1.5 cm in the plane transverse to the beam axis and 2.5 cm along the beam axis. The tracks used for the reconstruction of $\eta \rightarrow \pi^+\pi^-\pi^0$ must in addition have a transverse momentum p_T larger than 50 MeV/c. When PID criterion is required on a track, the track polar angle θ must be in the DIRC fiducial region $25.78° < \theta < 146.10°$. Photons are defined as single bumps in the EMC crystals not matched with any track, and with a shower lateral shape consistent with a photon. Because of high background in the forward region of the EMC caused by the beam asymmetry, the photons detected in the region $\theta < 21.19°$ are rejected.

Intermediate resonances of the decays $\overline{B}^0 \rightarrow D^{(*)0}h^0$ are reconstructed by combining tracks and/or photons for the channels with the highest decay rate and detection efficiency. When mesons are combined to build a resonance, masses are fixed to their nominal value [24]. For the ω and ρ^0 mesons, whose natural width is not negligible in comparison with the experimental resolution, their mass is not fixed to the nominal value. The selections applied to each meson π^0, η, ω, η', D^0, and D^{*0} are optimized by maximizing the figure of merit $S/\sqrt{S+B}$ where S is the number of signal and B is the number of background events. The numbers S and B are computed from simulations, the $\mathcal{BF}$'s used to evaluate S are the world average value given by PDG [24]. Each resonance mass distribution is fitted with a set of Gaussian functions or a *modified Novosibirsk*

function [29], which is composed of a Gaussian-like peaking part with two tails at low and high values. Resonance candidates are then required to have a mass within $\pm 2.5\ \sigma$ around the fitted mass central value, where σ is the resolution of the mass distribution obtained by the fit. For the resonances $D^0 \to K^-\pi^+\pi^0$ and $D^{*0} \to D^0\gamma$, the lower bound is extended to -3σ because of the photon energy losses in front and between the EMC crystals, which makes the mass distribution asymmetric with a tail at low values.

3.2 Selection of intermediate resonances

3.2.1 π^0 selection

The π^0 mesons are reconstructed by combining two photons, each photon energy $E(\gamma)$ must be larger than 85 MeV for π^0 coming from B^0 decay, and larger than 60 MeV for π^0 coming from η, ω or D^0. Soft π^0's coming from $D^{*0} \to D^0\pi^0$ must satisfy $E(\gamma) > 30$ MeV. The reconstruction resolution for high momentum π^0 is limited by the angle between the two daughter photons; for low momentum π^0 the resolution is limited by the neutral hadron background in EMC. The π^0 reconstructed mass resolution is about 6 MeV/c^2 for π^0 coming from η, 7 MeV/c^2 for π^0 coming from ω or D^0, and 8 MeV/c^2 for π^0 coming from B^0 or D^{*0}. The selection efficiency on signal ranges from 85 to 93 %.

3.2.2 η selection

The η mesons are reconstructed in the $\gamma\gamma$ and $\pi^+\pi^-\pi^0$ decay modes. These modes account for 62 % of the total decay rate [24], and may originate from $\overline{B}^0 \to D^{(*)0}\eta$ or $\eta' \to \pi^+\pi^-\eta$ decays.

The $\eta \to \gamma\gamma$ candidates are reconstructed by combining two photons that satisfy $E(\gamma) > 200$ MeV for $\overline{B}^0$ daughters and $E(\gamma) > 180$ MeV for η' daughters. As high momentum π^0s may fake $\eta \to \gamma\gamma$ decays, a veto is applied against π^0: for each $\eta \to \gamma_1\gamma_2$ candidate, the photons $\gamma_{1/2}$ are associated with photons of the rest of event γ_i. If $E(\gamma_i) > 200$ MeV and the invariant mass of the pair $\{\gamma_1\gamma_i\}$ or $\{\gamma_2\gamma_i\}$ is in the π^0 mass window $115 < m(\gamma_{1/2}\gamma_i) < 150$ MeV/c^2, then the η candidate is rejected. The resolution of the $\eta \to \gamma\gamma$ mass distribution is dominated by the EMC resolution and is about 15 MeV/c^2.

For η candidates reconstructed in $\pi^+\pi^-\pi^0$, the π^0 is required to satisfy the conditions described in Section 3.2.1. The mass resolution is about 3.5 MeV/c^2, which is smaller than for $\eta \to \gamma\gamma$ thanks to the higher resolution of the tracking system. The selection efficiency on signal is about 77 % for $\eta \to \gamma\gamma$ and 75 % for $\eta \to \pi^+\pi^-\pi^0$.

3.2.3 ω selection

The ω mesons are reconstructed in the $\pi^+\pi^-\pi^0$ decay mode. These modes account for 89 % of the total decay rate. The π^0s are required to satisfy the conditions described in Section 3.2.1 and the $\pi^\pm$ must fulfill the condition $p_T(\pi^\pm) > 200$ MeV/c. The natural width of the ω mass distribution $\Gamma \sim 8.49$ MeV [24] is comparable to the experimental resolution $\sigma \sim 7$ MeV/c^2, therefore the ω mass is not constrained to its nominal value. We define a total width $\sigma_{tot} = \sqrt{\sigma^2 + \Gamma^2} \sim 11$ MeV/c^2 and require the ω candidates to satisfy $|m(\omega) - m(\omega)_{\text{mean}}| < 2.5\ \sigma_{tot}$. The selection efficiency on signal is about 82 %.

3.2.4 ρ^0 selection

The ρ^0 mesons originate from $\eta' \to \rho^0 \gamma$ and are reconstructed in the $\pi^+\pi^-$ decay mode. These modes account for 100 % of the total decay rate. Charged particle tracks must satisfy $p_T(\pi^\pm) > 100$ MeV/c. We define the helicity angle θ_{ρ^0} as the angle between the pion momentum in the ρ^0 rest frame and the ρ^0 momentum in the η' rest frame. Because the ρ^0 is a vector and pion is a pseudoscalar, the angular distribution is proportional to $\sin(\theta_{\rho^0})^2$ for pure signal and is flat for background. The ρ^0 candidates with $|\cos(\theta_{\rho^0})| > 0.73$ are rejected. Due to the ρ^0 large natural width $\Gamma \sim 149.4$ MeV [24], no mass constraint is applied to the ρ^0. The mass of the ρ^0 candidates must be within 160 MeV/c^2 around the nominal mass value.

3.2.5 η' selection

The η' mesons are reconstructed in the $\pi^+\pi^-\eta(\to \gamma\gamma)$ and $\rho^0\gamma$ decay modes. These modes account for 30 % of the total decay rate. For the reconstruction of $\eta' \to \pi^+\pi^-\eta(\to \gamma\gamma)$, the η candidates must satisfy the selections described in Section 3.2.2. The η' mass resolution is about 3 MeV/c^2.

For η' candidates reconstructed in $\rho^0\gamma$, the ρ^0's are required to satisfy the conditions described in Section 3.2.4 and the photons must have an energy larger than 200 MeV. As photons coming from π^0 decays may fake signal, the veto against π^0 described in Section 3.2.2 is applied. The η' mass resolution is about 8 MeV/c^2, which is worse than $\eta' \to \pi^+\pi^-\eta$ because of the resolution on gamma reconstruction and the large ρ mass width.

The selection efficiency on signal is about 69 % for $\eta' \to \pi^+\pi^-\eta(\to \gamma\gamma)$ and 66 % for $\eta' \to \rho^0\gamma$.

3.2.6 K_S^0 selection

The K_S^0 mesons are reconstructed in the $\pi^-\pi^+$ decay modes. These modes account for 69 % of the total decay rate. The χ^2 probability of the vertex fit of charged pions must be larger than 0.1 %. We define the flight significance as the ratio L/σ_L where L is the K_S^0 flight length in the plane transverse to the beam axis and σ_L is the uncertainty on L determined from the vertex fit constraint. The combinatorial background is rejected by requiring a flight significance larger than 5. The reconstructed K_S^0 mass resolution is about 2 MeV/c^2. The selection efficiency on signal is about 86 %.

3.2.7 D^0 selection

The D^0 mesons are reconstructed in $K^-\pi^+$, $K^-\pi^+\pi^0$, $K^-\pi^+\pi^-\pi^+$, and $K_S^0\pi^+\pi^-$ decay modes. These modes account for about 28 % of the total decay rate. All D^0 candidates must satisfy $p^*(D^0) > 1.1$ GeV/c. That requirement is loose enough that background populate the sidebands of the signal region. The $\pi^\pm$'s coming from the D^0 candidate must fulfill $p_T(\pi^\pm) > 400$ MeV/c for $D^0 \to K^-\pi^+$, $p_T(\pi^\pm) > 100$ MeV/c for $D^0 \to K^-\pi^+\pi^-\pi^+$ and $p_T(\pi^\pm) > 120$ MeV/c for $D^0 \to K_S^0\pi^-\pi^+$. The χ^2 probability of the vertex fit of charged pions must be larger than 0.1 % for $D^0 \to K^-\pi^+$ and larger than 0.5 % for the other modes. The kaon candidates must satisfy tight kaon criteria for $K^-\pi^+$ and $K^-\pi^+\pi^0$, and a loose kaon criteria for $K^-\pi^+\pi^-\pi^+$. For $K_S^0\pi^+\pi^-$, the K_S^0 candidates must satisfy the selection criteria described in Section 3.2.6.

The decay D^0 to $K^-\pi^+\pi^0$ proceeds mainly through the resonances K^* ($K^{*0} \to K^-\pi^+$ or $K^{*-} \to K^-\pi^0$) and $\rho^+(\pi^+\pi^0)$. Combinatorial background is rejected by using the parametrization of the $K^-\pi^+\pi^0$ Dalitz distribution studied by the Fermilab E691 experiment [25]. The D^0 candidates

that are not in the resonance regions of the Dalitz distribution are rejected. The π^0 must satisfy the selections described in Section 3.2.1.

The reconstructed D^0 mass resolution is about 4, 5, 6, and 11 MeV/c^2 for $K^-\pi^+\pi^-\pi^+$, $K_S^0\pi^+\pi^-$, $K^-\pi^+$, and $K^-\pi^+\pi^0$ modes, respectively. To account for the asymmetry in the mass distribution of $D^0 \to K^-\pi^+\pi^0$, we require that the D^0 candidates satisfy $-3\,\sigma < (m(D^0) - m(D^0)_{\text{mean}}) < 2.5\,\sigma$.

The selection efficiency on signal is about 71 % for $K^-\pi^+$, 60 % for $K^-\pi^+\pi^-\pi^+$, 71 % for $K_S^0\pi^+\pi^-$, and 44 % for $K^-\pi^+\pi^0$.

3.2.8 D^{*0} selection

The D^{*0} mesons are reconstructed in the $D^0\pi^0$ and $D^0\gamma$ decay modes. The π^0 and D^0 candidates are required to satisfy the selections described in Section 3.2.1 and 3.2.7 respectively. The photons from $D^{*0} \to D^0\gamma$ must fulfill $E(\gamma) > 200$ MeV and pass the veto against π^0 described in Section 3.2.2.

The resolution of the mass difference $\Delta m \equiv m(D^{*0}) - m(D^0)$ is about 2 MeV/c^2 for $D^0\pi^0$ and 7 MeV/c^2 for $D^0\gamma$. The $D^{*0} \to D^0\pi^0$ candidates must satisfy $|\Delta m - \Delta m_{\text{mean}}| < 2.5\,\sigma$. Because of the asymmetry of the Δm distribution for $D^0\gamma$, the D^{*0} candidates must satisfy $-3\,\sigma < (\Delta m - \Delta m_{\text{mean}}) < 2.5\,\sigma$.

The selection efficiency on signal is about 49 % for $D^0\pi^0$ and 39 % for $D^0\gamma$.

3.3   Selection of B candidates

The B candidates are reconstructed by combining a $D^{(*)0}$ with an h^0, with the D^{*0} and h^0 masses constrained to their nominal value except when h^0 is the ω. One needs to discriminate real B's from fake ones created from combinatorial or crossfeed background.

3.3.1 B kinematic variables

Two kinematic variables are used in *BABAR* to select B candidates: the energy-substituted mass m_{ES} and the energy difference ΔE. These two variables use the constraints from the precise knowledge of the beams' energies and from energy conservation in the two-body decay $\Upsilon(4S) \to B\overline{B}$. The quantity m_{ES} is the invariant mass of the B candidate where the B energy is set to the beam energy in the CM frame:

$$m_{\text{ES}} = \sqrt{\left(\frac{\sqrt{s}}{2}\right)^2 - |\overrightarrow{p_B^*}|^2}, \tag{1}$$

and ΔE is the energy difference between the reconstructed B energy and the beam energy in the CM frame:

$$\Delta E = E_B^* - \sqrt{s}/2, \tag{2}$$

where $\sqrt{s}$ is the e^+e^- CM energy and $(E_B^*, \overrightarrow{p_B})$ is the B quadrivector in the CM frame. For B signal events, the m_{ES} distribution peaks at the B mass with a resolution of about 3 MeV/c^2 dominated by the beam energy spread, whereas ΔE peaks near zero with a resolution of $15 - 50$ MeV depending on the number of photons in the final state.

3.3.2 Rejection of $e^+e^- \to q\bar{q}$ background

The continuum background $e^+e^- \to q\bar{q}$ ($q = u$, d, s or mainly c) creates real high momentum mesons $D^{(*)0}$, π^0, $\eta^{(')}$, ω that can fake the signal mesons originating from the two body decays $\overline{B}^0 \to D^{(*)0}h^0$. That background is thus not rejected by the selections on intermediate resonances. Since the B mesons are produced almost at rest in the $\Upsilon(4S)$ frame, so the $\Upsilon(4S) \to B\overline{B}$ events shape is spherical. By comparison, the $q\bar{q}$ events have a back-to-back jet-like shape given that the quark masses ($q \neq b$) are small compared to the CM energy. The $q\bar{q}$ background can hence be discriminated by the event shape described by the following variables:

- The thrust angle θ_T defined as the angle between the thrust axis of the B candidate and the thrust axis of the rest of event. The thrust axis $\widehat{T}$ is defined as the axis that maximizes the quantity T:

$$T = \frac{\sum_i |\overrightarrow{p_i} \cdot \widehat{T}|}{\sum_i |\overrightarrow{p_i}|}. \tag{3}$$

  The distribution of $|\cos(\theta_T)|$ is flat for signal and peaks at 1 for continuum background.

- Legendre monomials L_0 and L_2 defined as:

$$L_0 = \sum_i p_i^* \; ; \; L_2 = \sum_i p_i^* |\cos(\theta_i^*)|^2, \tag{4}$$

  with p_i^* the momentum of the particle i that does not come from a B candidate, and θ_i^* is the angle between p_i^* and the thrust axis of the B candidate.

- The polar angle θ_B^* between the B momentum in the $\Upsilon(4S)$ frame and the beam axis. The $\Upsilon(4S)$ being vector ($J = 1$) and the B mesons being pseudoscalar ($J = 0$), the angular distribution is proportional to $\sin^2(\theta_B^*)$ for signal and roughly flat for background.

These four variables are combined in a Fisher discriminant built with the TMVA [26] toolkit package. The Fisher $\mathcal{F}_{shape}$ is trained with signal MC events and off-peak data events; in order to maximize the number of off-peak events all the $\overline{B}^0 \to D^{(*)0}h^0$ modes are combined. The training and test are performed with 2×20000 signal events and 2×20000 off-peak events. The obtained Fisher formula is:

$$\begin{aligned} \mathcal{F}_{shape} = 2.36 - 1.18 \cdot |\cos(\theta_T)| + \\ 0.20 \cdot L_0 - 1.01 \cdot L_2 - 0.80 \cdot |\cos(\theta_B^*)|. \end{aligned} \tag{5}$$

The $q\bar{q}$ background is rejected by applying a selection on $\mathcal{F}_{shape}$. The selection is optimized for each $\overline{B}^0$ signal mode by maximizing the statistical significance with signal MC against generic MC $e^+e^- \to q\bar{q}$, $q \neq b$. That requirement retains between 36 % and 98 % of B signal, while rejecting between 23% and 97 % of the $q\bar{q}$ background respectively.

3.3.3 Rejection of $\Upsilon(4S) \to B\overline{B}$ background

The ω mesons in $\overline{B}^0 \to D^0\omega$ are polarized. We define the *normal angle* θ_N [9, 32] as the angle between the normal to the ω decay plane and the direction of $\overline{B}^0$ in the ω rest frame. That definition is the equivalent of the two-body helicity angle for the three-body decay. To describe the 3-body

decay distribution of $\omega \to \pi^+\pi^-\pi^0$, we define the *Dalitz angle* θ_D [9] as the angle between the π^0 momentum in the ω frame and the π^+ momentum in the $\{\pi^+\pi^-\}$ frame.

Given the angular momenta of the $\overline{B}^0$ and D^0 mesons $(J = 0)$, and ω meson $(J = 1)$, the signal distribution is proportional to $\cos^2(\theta_N)$ and $\sin^2(\theta_D)$ while the combinatorial background distribution is roughly flat. These two angles are combined in a Fisher discriminant $\mathcal{F}_{hel}$ built from signal MC events and generic $q\overline{q}$ and $B\overline{B}$ MC events:

$$\mathcal{F}_{hel} = -1.41 - 1.01 \cdot |\cos(\theta_D)| + 3.03 \cdot |\cos(\theta_N)|. \tag{6}$$

We require $\overline{B}^0 \to D^0\omega$ candidates to satisfy $\mathcal{F}_{hel} > -0.1$, to obtain an efficiency on signal (background) of 85 % (39 %).

We also use the angular distribution of $D^{*0} \to D^0\pi^0$ to reject combinatorial background. We define the helicity angle θ_{D*} as the angle between the D^0 momentum in the D^{*0} frame and the D^{*0} momentum in the $\overline{B}^0$ frame. The angular distribution is proportional to $\cos(\theta_{D*})^2$ for signal and roughly flat for combinatorial background. Selection on $|\cos(\theta_{D*})|$ significantly improves the statistical significance for the $\overline{B}^0 \to D^{*0}\pi^0$ mode only. The D^{*0} candidates coming from the decay $\overline{B}^0 \to D^{*0}\pi^0$ are then required to satisfy $|\cos(\theta_{D*})| > 0.4$ for an efficiency on signal of 90 % and on background of 62 %.

An important $B\overline{B}$ background contribution in the reconstruction of $\overline{B}^0 \to D^{(*)0}\pi^0$ comes from the color-allowed decay $B^- \to D^{(*)0}\rho^-$. If the charged pion from the decay $\rho^- \to \pi^-\pi^0$ is not used in the construction of the B candidate, $D^{(*)0}\rho^-$ events mimic the $D^{(*)0}\pi^0$ signal. Moreover, the $\mathcal{BF}$ of $B^- \to D^{(*)0}\rho^-$ is almost 50 times larger than the signal $\mathcal{BF}$, and is known with a relative total uncertainty of 13 % for $D^0\rho^-$ and 17 % for $D^{*0}\rho^-$ [24]. A veto is applied against $B^- \to D^{(*)0}\rho^-$ events. For each $D^{(*)0}\pi^0$ candidate, a B^- candidate is reconstructed in $D^{(*)0}\rho^-$. If the B^- candidate mass is in the signal region $m_{\mathrm{ES}}(B^-) > 5.27$ GeV/c^2, $|\Delta E(B^-)| < 100$ MeV and $|m(\rho^-) - m(\rho^-)_{\mathrm{PDG}}| < 250$ MeV/c^2, and if the π^0 and D^0 candidates are the same used to build the $\overline{B}^0$ candidate, then the $\overline{B}^0$ is rejected. For the reconstruction of $D^0\pi^0$, the veto retains about 90 % of signal and rejects about 67 % of $D^0\rho^-$ and 44 % of $D^{*0}\rho^-$. For the reconstruction of $D^{*0}\pi^0$, the veto efficiency on signal is 80 % while rejecting about 56 and 66 % on $D^0\rho^-$ and $D^{*0}\rho^-$ respectively.

3.3.4 Choice of one B candidate

The average number of B candidate per event after all selections ranges between 1 and 1.6 depending on the subdecays. The highest multiplicities correspond to modes with the largest number of neutral particles in the final state. We keep one B candidate per mode per event. The chosen B is the one with the smaller value of:

$$\begin{aligned} \chi_m^2 \quad &= \quad \left(\frac{m(D^0) - m(D^0)_{\mathrm{mean}}}{\sigma_{m(D^0)}}\right)^2 \\ &+ \quad \left(\frac{m(h^0) - m(h^0)_{\mathrm{mean}}}{\sigma_{m(h^0)}}\right)^2, \end{aligned} \tag{7}$$

for D^0h^0 modes and

$$\chi_m^2 = \left(\frac{m(D^0) - m(D^0)_{\text{mean}}}{\sigma_{m(D^0)}}\right)^2$$

$$+ \left(\frac{m(h^0) - m(h^0)_{\text{mean}}}{\sigma_{m(h^0)}}\right)^2$$

$$+ \left(\frac{\Delta m - \Delta m_{\text{mean}}}{\sigma_{\Delta m}}\right)^2, \tag{8}$$

for the $D^{*0}h^0$ modes. The quantities $\sigma_{m_{D^0}}$ and $\sigma_{m_{h^0}}$ (with respect to $m(D^0)_{\text{mean}}$ and $m(h^0)_{\text{mean}}$) are the resolutions (with respect to means) of the reconstructed mass distributions. The quantities Δm_{mean} and $\sigma_{\Delta m}$ are respectively the mean and resolution of the Δm distribution. These quantities are obtained from fits of the mass distribution of true simulated candidates selected from signal MC simulations. An associated systematic error is calculated later because of the use of MC to calculate Δm_{mean} and $\sigma_{\Delta m}$. The efficiency on signal of the choice of one B per event ranges from 76 to 100 %. The lower efficiencies correspond to the modes with high neutral multiplicity.

3.3.5   MC efficiency corrections

The branching fraction is computed as:

$$\mathcal{BF} = \frac{S}{n_{B\bar{B}} \cdot \epsilon \cdot \mathcal{BF}_{sec}}, \tag{9}$$

where $\mathcal{BF}_{sec}$ is the product of the $\mathcal{BF}$'s of the intermediate resonances reconstructed decays, which are taken from the PDG [24], $n_{B\bar{B}}$ is the number of $B\bar{B}$ pairs in data and S is the number of signal events remaining after all selections. The quantity ϵ is the signal efficiency of reconstruction and selections, computed from the exclusive MC simulations, and the quantity $\epsilon \cdot \mathcal{BF}_{sec}$ is the total acceptance. When computing the $\mathcal{BF}$ of the sum of $D^{(*)0}$ subdecays, the corresponding total acceptances are summed. The total acceptance is corrected by about 1 % (10 %) from the crossfeed between D^0 (D^{*0}) decay modes. The high correction for the sum of D^{*0} decays is mainly due to the large crossfeed of $D^{*0} \rightarrow D^0\pi^0$ into $D^{*0} \rightarrow D^0\gamma$. That correction was obtained by computing with exclusive MC's the proportion of intern crossfeed by respect to real signal.

The selection efficiency from simulation is slightly different from the efficiency in data. The MC efficiency for the reconstruction of π^0/γ is adjusted from the study of τ decays in the channels $\tau \rightarrow \rho(\pi\pi^0)\nu_\tau$ and $\tau \rightarrow \pi\nu_\tau$ [27]. The correction on track efficiency is computed from studies of track mis-reconstruction in the decays $\tau \rightarrow (\pi^+\pi^-)\pi^-\nu_\tau$ and $\tau \rightarrow \rho^0(\pi^+\pi^-)\pi^-\nu_\tau$ [28]. The simulated efficiency of charged particle identification is compared to the efficiency computed in data with pure samples of kaons from the decays $D^{*+} \rightarrow D^0\pi^+$ and $D^0 \rightarrow K^-\pi^+$. The efficiency on K_S^0 candidates is modified using a high statistics and a high purity data sample of K_S^0 mainly arising from the process $e^+e^- \rightarrow q\bar{q}$.

The efficiency corrections for the selections applied to $D^{(*)0}$ candidates and on the Fisher discriminant for the $q\bar{q}$ rejection are obtained from the study of the control sample $B^- \rightarrow D^{(*)0}\pi^-$. That control sample was chosen for its high statistics and purity, and for its similarity with $\bar{B}^0 \rightarrow D^{(*)0}h^0$. The correction is computed from the double ratio eff(data)/eff(MC), where the efficiencies are computed from m_{ES} fits of $B^- \rightarrow D^{(*)0}\pi^-$ events in data and MC, before and after the corresponding selections. The obtained results were checked with the color-allowed control sample

$B^- \to D^{(*)0}\rho^-$ which has a slightly different kinematic due to the mass of the ρ^- and validates this correction for modes as $D^{(*)0}\eta'$.

3.4 Probability density functions (pdf) and fit procedure

The signal yield S is extracted by an extended unbinned maximum likelihood (ML) fit of the ΔE distribution in the range $-0.280 < \Delta E < 0.280$ GeV for $m_{\mathrm{ES}} > 5.27$ GeV/c^2. Fitting ΔE allows us to model and to fit the complex crossfeed structure without relying on simulation completely.

Due to the energy loss by photons in the detector material before the EMC, the ΔE distribution for signal is modelled by a modified Novosibirsk function [29]. A Gaussian is added to the modes with a large ΔE resolution to describe the mis-reconstructed events. The signal shape parameters are estimated from a ML fit of simulated signal events in exclusive decay modes.

The dominant crossfeed contribution for $\overline{B}^0 \to D^0 h^0$ comes from the channel $\overline{B}^0 \to D^{*0} h^0$ when the π^0/γ from the D^{*0} decay is not reconstructed. Such crossfeed events are shifted in ΔE by about -135 MeV with a tail from $D^{*0}(\to D^0\gamma)h^0$ in the signal region.

Table 1: Main crossfeed between signal modes.

B mode	Crossfeed mode
$D^0 h^0$	$D^{*0} h^0$
$D^{*0}(D^0\pi^0)h^0$	$D^{*0}(D^0\gamma)h^0$, $D^0 h^0$
$D^{*0}(D^0\gamma)h^0$	$D^{*0}(D^0\pi^0)h^0$, $D^0 h^0$
$D^{*0} h^0$	$D^0 h^0$

The main crossfeed contributions from the other reconstructed B^0 modes are shown in Table 1. For each signal mode, different crossfeeds are summed and their contribution is estimated with a histogram-based pdf built from the signal MC. The major crossfeed in the reconstruction of $\overline{B}^0 \to D^{(*)0}\pi^0$ comes from the decays $B^- \to D^{(*)0}\rho^-$ (see Section 3.3.3). Their contribution is modelled by a separate histogram-based pdf built from the exclusive MC simulations.

The combinatorial background from $B\overline{B}$ and $q\overline{q}$ are summed and modelled by a 2nd order polynomial. In the cases of $\overline{B}^0 \to D^{(*)0}\omega(\eta)$ modes, an additional crossfeed contribution comes respectively from the decays $B^- \to D^{(*)0}\pi^-\omega(\eta)$. In the reconstruction of $\overline{B}^0 \to D^0\pi^0$ where all D^0 subdecays are summed, an additional crossfeed contribution comes mainly from the decays $B^- \to D^0\rho^-$, $\overline{B}^0 \to D^0\pi^0\pi^0$, $\overline{B}^0 \to \overline{K}^{*0}\pi^0\pi^0$ and $\overline{B}^0 \to D^0\pi^0$ where D^0 decays to a CP eigenstate or through a semileptonic channel. These peaking backgrounds are significant when summing the D^0 submodes. In these cases, the combinatorial background is modelled by a first-order polynomial plus a Gaussian to take into account additional crossfeeds. For $\overline{B}^0 \to D^{(*)0}\omega(\eta)$ modes, the fraction of that Gaussian is left floating in the fit, since the $\mathcal{BF}$'s of $B^- \to D^{(*)0}\pi^-\omega(\eta)$ are not precisely known.

The shape parameters of the combinatorial background pdf are obtained from ML fits on the $B\overline{B}$ and continuum MC, where all signal and crossfeed events have been removed.

The pdf normalization for the signal, for the combinatorial background and for the crossfeed $D^{(*)0}\rho^-$ are allowed to float in the fit. The mean of the signal pdf is left floating for the sum of $D^{(*)0}$ subdecays. For each D^0 submodes the signal mean is fixed to the value obtained with the fit on the sum of D^0 submodes.

A given mode $\overline{B}^0 \to D^{*0}h^0$ can be signal and crossfeed to other modes at the same time. In order to use the $\mathcal{BF}$ computed in this analysis, the yield extraction is performed through an iterative fit on successively $D^{*0}h^0$ and D^0h^0. The normalization of crossfeed contribution from $D^{(*)0}h^0$ is then fixed to the $\mathcal{BF}$ measured in the previous fit iteration. That iterative method converges quickly to a stable value of $\mathcal{BF}$, with variation below 10 % of statistical uncertainty, in less than 5 iterations.

We check the absence of bias in our fit by studying embedded toy MC's. The extraction procedure is applied to toy samples where background events are generated from the fitted pdf's. The toy signal events are taken from the corresponding exclusive MC with a yield corresponding to the MC-generated value of the branching fraction $\mathcal{BF}_{gen}$. No significant bias are found.

3.5 Signal yield extraction

The iterative fit procedure is applied to data. The fitted ΔE distributions for the sum of $D^{(*)0}$ submodes are given in Figures 2 and 3.
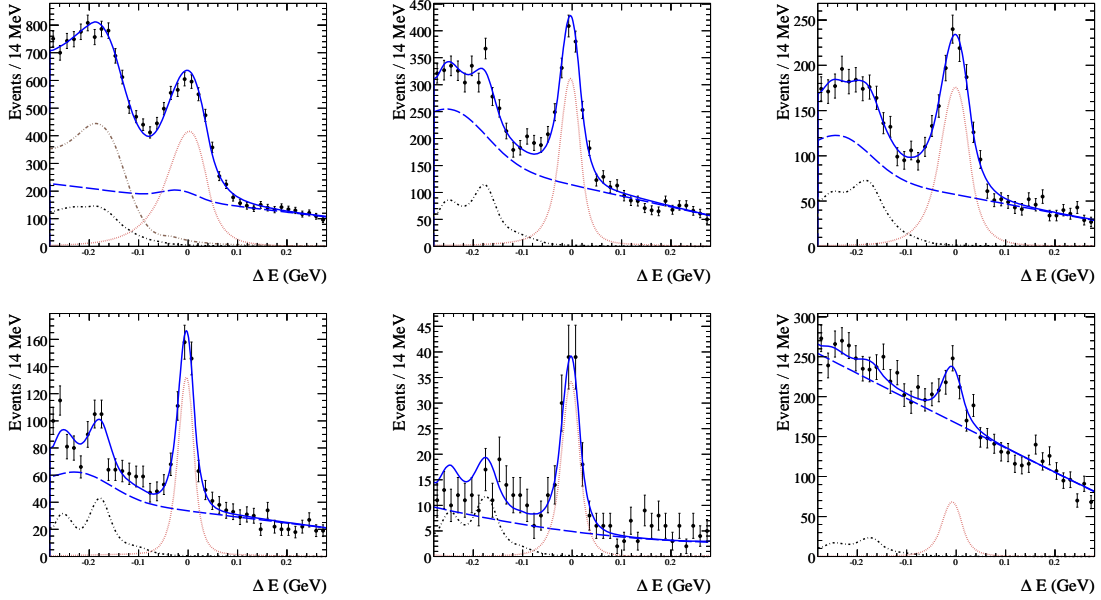

Figure 2: Fit of ΔE distributions in data for modes $\overline{B}^0 \to D^0\pi^0$ (top left), $\overline{B}^0 \to D^0\omega$ (top middle), $\overline{B}^0 \to D^0\eta(\gamma\gamma)$ (top right), $\overline{B}^0 \to D^0\eta(\pi\pi\pi^0)$ (bottom left), $\overline{B}^0 \to D^0\eta'(\pi\pi\eta)$ (bottom middle) and $\overline{B}^0 \to D^0\eta'(\rho^0\gamma)$ (bottom right). The dots with error bars are data, the solid curve is the fitted total pdf, the dotted curve is the signal pdf, the dotted-dashed curve is the crossfeed pdf, the double dotted-dashed curve is the $B^- \to D^{(*)0}\rho^-$ pdf and the long dashed curve is the combinatorial background pdf.

The signal and background yields obtained from the fit to data are given in Table 2 with the corresponding statistical significances.
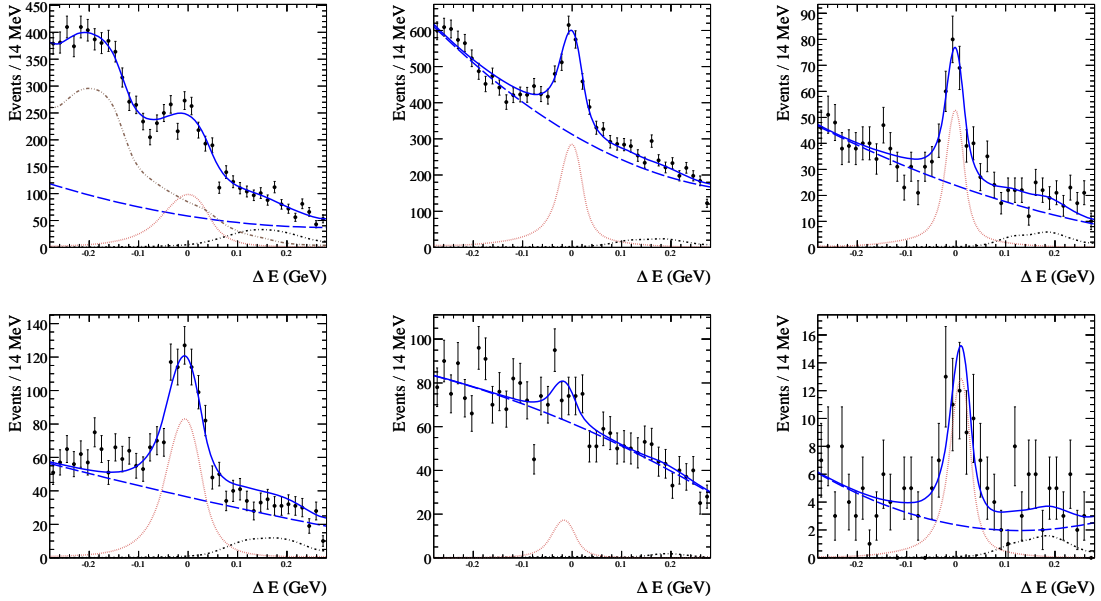
17

Figure 3: Fit of ΔE distributions in data for modes $\overline{B}^0 \to D^{*0}\pi^0$ (top left), $\overline{B}^0 \to D^{*0}\omega$ (top middle), $\overline{B}^0 \to D^{*0}\eta(\pi\pi\pi^0)$ (top right), $\overline{B}^0 \to D^{*0}\eta(\gamma\gamma)$ (bottom left), $\overline{B}^0 \to D^{*0}(D^0\pi^0)\eta'(\rho^0\gamma)$ (bottom middle) and $\overline{B}^0 \to D^{*0}\eta'(\pi\pi\eta)$ (bottom right). Detailed legend is provided in Figure 2.

4   SYSTEMATIC STUDIES

There are several sources of systematic uncertainty in this analysis. Table 3 summarizes the studied systematic uncertainties with their values in percentage of $\mathcal{BF}$ for the different modes $D^{(*)0}h^0$. The large uncertainties for $D^{*0}h^0$ mainly come from $D^{*0}(D^0\gamma)h^0$.

The categories "π^0/γ detection" ("Tracking") account for the systematics on the reconstruction of π^0/γ and charged particle tracks, and are taken as the uncertainty on the efficiency correction computed in the study of τ decays (see Section 3.3.5).

Similarly, the systematic uncertainties on kaon identification and K_S^0 selections, are estimated from the uncertainties on MC efficiency corrections computed in the study of pure samples of kaons and K_S^0 mesons in data respectively (see Section 3.3.5).

The systematic errors on the submodes $\mathcal{BF}$ is a combination of the uncertainty on each D^0 and h^0 submode [24]. The correlation between the calibration mode $D^0 \to K^-\pi^+$ and $D^0 \to X$, $X \neq K^-\pi^+$ was accounted for.

The uncertainty related to the number of $B\overline{B}$ pairs and to the limited MC statistics is also included [9].

The systematics on resonance mass cut are computed as the relative difference of signal yield when the mass mean and resolution for the selection are taken from a fit in data.

The uncertainties for the $q\overline{q}$ rejection and the $D^{(*)0}$ selections are obtained from the study performed on the control sample $B^- \to D^{(*)0}\pi^-$ and are estimated as the uncertainty on the efficiency correction eff(data)/eff(MC), including the correlations between the samples before and after selections (see Section 3.3.5).

The uncertainties for the cuts on ρ^0 and $D^0\omega$ helicities are obtained by varying the selection

Table 2: We give the number of signal events (S), crossfeed (N_{cf}), $B^- \to D^{(*)0}\rho^-$ ($N_{\mathrm{D}\rho}$) and combinatorial background (N_{combi}) from the ΔE fit of data, and the $\mathcal{BF}$ measured for each submode. The number of background events N_{cf}, $N_{\mathrm{D}\rho}$, and N_{combi} are computed from the fitted pdf in the window $|\Delta E| < 100$ MeV. The *statistical significance* is defined as $\sqrt{2ln(L_{S+B}/L_B)}$, where L_{S+B} is the likelihood of the fit in data for the hypothesis of a signal, while L_B is the likelihood for the hypothesis of pure background only.

$\overline{B}^0$ mode (decay channel)	S	N_{cf}	$N_{\mathrm{D}\rho}$	N_{combi}	$\mathcal{BF}(\times 10^{-4})$ ±stat. ± syst.	Statistical significance
$D^0\pi^0$	3369 ± 102	135	440 ± 11	2585 ± 63	$2.78 \pm 0.08 \pm 0.20$	35.5
$D^0\eta(\gamma\gamma)$	1054 ± 49	44	-	823 ± 21	$2.34 \pm 0.11 \pm 0.17$	26.1
$D^0\eta(\pi\pi\pi^0)$	454 ± 29	20	-	487 ± 15	$2.51 \pm 0.16 \pm 0.17$	20.3
$D^0\omega$	1400 ± 58	68	-	1648 ± 28	$2.77 \pm 0.13 \pm 0.22$	29.4
$D^0\eta'(\pi\pi\eta(\gamma\gamma))$	134 ± 14	6	-	74 ± 6	$1.29 \pm 0.14 \pm 0.09$	14.7
$D^0\eta'(\rho^0\gamma)$	290 ± 42	13	-	2382 ± 33	$1.95 \pm 0.29 \pm 0.30$	7.2
$D^{*0}\pi^0$	958 ± 73	121	1218 ± 41	844 ± 56	$1.78 \pm 0.13 \pm 0.23$	15.1
$D^{*0}\eta(\gamma\gamma)$	629 ± 39	33	-	525 ± 18	$2.37 \pm 0.15 \pm 0.24$	19.4
$D^{*0}\eta(\pi\pi\pi^0)$	241 ± 25	11	-	341 ± 13	$2.27 \pm 0.23 \pm 0.18$	12.2
$D^{*0}\omega$	1692 ± 86	60	-	4507 ± 47	$4.44 \pm 0.23 \pm 0.61$	22.3
$D^{*0}\eta'(\pi\pi\eta)$	61 ± 10	3	-	34 ± 4	$1.12 \pm 0.26 \pm 0.27$	8.0
$D^{*0}(D^0\pi^0)\eta'(\rho^0\gamma)$	86 ± 28	6	-	874 ± 20	$1.64 \pm 0.53 \pm 0.20$	3.3

cut values by ± 10 % around the maximum of statistical significance.

The category "Signal shape" represents the uncertainty on the shape of the signal pdf for the ΔE fit. The expected shape difference between data and MC is estimated from a study of the control sample $B^- \to D^{(*)0}\rho^-$, hich gives: $|\Delta\mathrm{mean}| \simeq 5.7$ MeV and $|\Delta\sigma| \simeq 2.3$ MeV. The systematic on signal shape is obtained by varying the pdf parameters by ± 5.7 MeV for the mean and ± 2.3 MeV for the resolution.

The uncertainty on the continuum background shape is estimated from the difference of the pdf fitted on generic MC's with the pdf fitted in the m_{ES} sideband $5.24 < m_{\mathrm{ES}} < 5.26$ GeV/c^2 in data. When a Gaussian is added to the combinatorial background shape, the related uncertainty is computed by varying its means and resolution by $\pm 1\sigma$.

The uncertainties related to the branching fractions of the crossfeed from $D^{(*)0}h^0$ and $D^{(*)0}\rho^-$ were computed by varying the $\mathcal{BF}$ separately by $\pm 1\sigma$ in the fit procedure. The value of σ used is taken from the fit for $D^{(*)0}h^0$ and from PDG for $D^{(*)0}\rho^-$.

The uncertainty related to the crossfeed shape, modelled by a non-parametric pdf, is obtained by shifting and smearing the pdf mean and resolution by ± 5.7 and 2.3 MeV respectively, with a convolution by a Gaussian.

The uncertainty in "$D^{*0}\omega$ helicity" accounts for the hypothesis on the $D^{*0}\omega$ polarization in the MC generation. As that polarization had never been measured, following HQET and factorization based arguments, the $D^{*0}\omega$ polarization was simulated using the helicity parameters measured in $B^- \to D^{*0}\rho^-$, thus a longitudinal fraction of $f_L = 0.869$ [30], confirmed by a CLEO measurement [31]. That systematic is estimated by a comparison of the efficiency as obtained from an exclusive simulation of $\overline{B}^0 \to D^{*0}\omega$ with a low f_L value of 0.08 and is taken as half of the relative difference of the signal yield.

The most significant systematic uncertainties come from the π^0/γ reconstruction, the submodes

$\mathcal{BF}$, the longitudinal fraction for $D^{*0}\omega$, from the signal and background parametrization on the ΔE fit and from the crossfeed by $D^{(*)0}\rho^-$.

Table 3: Systematic uncertainties (%) for the modes $\overline{B}^0 \to D^{(*)0}h^0$ where $D^{(*)0}$ submodes are summed.

Sources	D^0h^0						$D^{*0}h^0$					
	π^0	$\eta(\gamma\gamma)$	$\eta(3\pi)$	ω	$\eta'(\pi\pi\eta)$	$\eta'(\rho^0\gamma)$	π^0	$\eta(\gamma\gamma)$	$\eta(3\pi)$	ω	$\eta'(\pi\pi\eta)$	$\eta'(\rho^0\gamma)$
π^0/γ detection	4.0	4.0	4.0	4.0	4.0	2.4	5.9	5.9	6.1	6.1	5.8	4.5
PID	1.1	1.1	1.2	1.2	1.2	1.1	1.2	1.2	1.2	1.2	1.2	1.2
Tracking	0.9	0.9	1.6	1.6	1.6	1.6	0.9	0.9	1.6	1.6	1.5	1.5
K_S^0 selection	0.1	0.1	0.1	0.1	0.1	0.1	0.0	0.1	0.0	0.1	-	-
Submodes $\mathcal{BF}$	3.2	3.3	3.5	3.3	4.5	4.4	3.1	3.2	3.4	3.2	4.3	6.4
$B\overline{B}$ counting	1.1	1.1	1.1	1.1	1.1	1.1	1.1	1.1	1.1	1.1	1.1	1.1
MC statistics	0.3	0.5	0.7	0.4	1.0	0.9	0.6	0.8	1.1	0.6	1.1	1.2
Resonances mass	0.5	0.7	0.4	0.1	0.7	0.7	0.5	0.7	0.4	0.1	0.7	0.7
$q\overline{q}$ rejection	0.2	0.2	0.2	0.2	0.2	0.2	0.2	0.2	0.2	0.2	0.2	0.2
$D^{(*)0}$ selection	0.3	0.3	0.3	0.3	0.3	0.3	0.4	0.4	0.4	0.4	0.4	0.4
ρ^0 helicity	-	-	-	-	-	2.1	-	-	-	-	-	2.1
$D^{(*)0}\omega$ helicity	-	-	-	1.9	-	-	-	-	-	10.8	-	-
Signal shape	2.6	2.8	1.5	1.7	1.3	2.7	1.9	2.8	1.8	3.3	1.0	3.1
Continuum shape	1.0	0.8	1.1	4.2	1.2	13.3	0.9	6.5	1.7	3.3	21.2	6.8
Crossfeed $\mathcal{BF}$	0.0	0.0	0.0	0.0	0.1	0.1	8.6	1.2	2.11	0.8	8.6	0.3
Crossfeed shape	0.7	0.7	0.3	0.6	0.5	0.4	6.1	0.2	0.3	0.2	0.6	0.2
Total	6.2	6.3	6.2	7.5	6.8	14.9	12.8	10.0	8.1	13.8	24.1	11.3

5 RESULTS

5.1 $\mathcal{BF}$ measurement

The branching fractions obtained from the ΔE fit on data are given in Table 2 for the sum of the $D^{(*)0}$ submodes. The consistency with D^0 submodes was checked. All the quoted results are the branching fraction $\mathcal{BF}_{\text{sum}}$ computed with the fit of the D^0 sum.

The statistical uncertainty σ_{stat} on $\mathcal{BF}_{\text{sum}}$ is provided by the fit while the systematic uncertainty is computed as the average of the systematic weighted by the total corrected acceptance $\mathcal{A}_i$:

$$\sigma_{\text{syst}} = \frac{\sum_i \mathcal{A}_i \cdot \sigma_{\text{syst},i}}{\sum_i \mathcal{A}_i}, \tag{10}$$

where $(\mathcal{BF}_i \pm \sigma_{\text{syst},i} \pm \sigma_{\text{stat},i})$ is the measured branching fraction with the submode $i = K^-\pi^+$, $K^-\pi^+\pi^-\pi^+$, $K^-\pi^+\pi^0$ or $K_S^0\pi^+\pi^-$. The total uncertainty is eventually computed as the quadrature sum of σ_{stat} and σ_{syst}. We checked the compatibility of $\mathcal{BF}_{\text{sum}}$ with the measurements in the submodes $\mathcal{BF}_i$ for significant signal. The $\mathcal{BF}$'s measured with D^{*0} submodes are compatible with $\mathcal{BF}_{\text{sum}}$, except for $\overline{B}^0 \to D^{*0}\pi^0$ where the incompatibility between $D^{*0} \to D^0\gamma$ and $D^{*0} \to D^0\pi^0$ is due to the large background contribution from $D^{(*)0}\rho^-$. Likewise the measurements in the different η or η' submodes are compatible. The measurements in the $\eta^{(')}$ submodes are combined through a $\mathcal{BF}$ average weighted by the total uncertainty on $\mathcal{BF}$:

$$\mathcal{BF}_{\mathrm{avg}} = \frac{\sum_i \mathcal{BF}_i/\sigma_i^2}{\sum_i 1/\sigma_i^2}, \qquad (11)$$

where $(\mathcal{BF}_i \pm \sigma_i)$ is the measured branching fraction with the submode i, and σ_i the total uncertainty on $\mathcal{BF}_i$. The statistical uncertainty on the $\mathcal{BF}$ combination is :

$$\sigma_{\mathrm{stat,avg}}^2 = \sum_i \frac{1}{1/\sigma_{\mathrm{stat},i}^2}, \qquad (12)$$

and the systematic is obtained from the Equation (10).

The $\mathcal{BF}$'s measured in this analysis are compatible with the previous measurements by BABAR [9], CLEO [7] and Belle [10, 11]. For the modes $\overline{B}^0 \to D^{(*)0}\eta$, $D^{*0}\omega$ and $D^{*0}(D^0\pi^0)\pi^0$,

our measured $\mathcal{BF}$s are significantly higher than the ones measured by Belle [11]. We also measured the $\mathcal{BF}$ in the dataset studied previously by BABAR [9] and found compatible $\mathcal{BF}$ values with systematic uncertainties lowered by about 25 to 50 %. The improvement mainly comes from the selections on $D^{(*)0}$ and on the $q\bar{q}$ background rejection.

5.2 Isospin analysis

The isospin I symmetry relates the amplitudes of the decays $B^- \to D^{(*)0}\pi^-$, $\overline{B}^0 \to D^{(*)+}\pi^-$ and $\overline{B}^0 \to D^{(*)0}\pi^0$, which can be written as linear combinations of the isospin eigenstates $\mathcal{A}_I$, $I = 1/2$, $3/2$ [4, 33]:

$$\begin{aligned}
\mathcal{A}(D^{(*)0}\pi^-) &= \sqrt{3}\mathcal{A}_{3/2,D^{(*)}}, \\
\mathcal{A}(D^{(*)+}\pi^-) &= 1/\sqrt{3}\mathcal{A}_{3/2,D^{(*)}} + \sqrt{2/3}\mathcal{A}_{1/2,D^{(*)}}, \\
\mathcal{A}(D^{(*)0}\pi^0) &= \sqrt{2/3}\mathcal{A}_{3/2,D^{(*)}} - \sqrt{1/3}\mathcal{A}_{1/2,D^{(*)}},
\end{aligned} \qquad (13)$$

and so:

$$\mathcal{A}(D^{(*)0}\pi^-) = \mathcal{A}(D^{(*)+}\pi^-) + \sqrt{2}\mathcal{A}(D^{(*)0}\pi^0). \qquad (14)$$

The relative strong phase between the eigenstates $\mathcal{A}_{1/2}$ and $\mathcal{A}_{3/2}$ is noted as δ for the $D\pi$ system and δ^* for $D^*\pi$ system. Final State Interactions between the states $D^{(*)0}\pi^0$ and $D^{(*)+}\pi^-$ may lead to a value of $\delta^{(*)}$ different from zero and, through constructive interference, to a higher value of $\mathcal{BF}$ for $D^{(*)0}\pi^0$. One can also define the amplitude ratio $R^{(*)}$:

$$R^{(*)} = \frac{|\mathcal{A}_{1/2}^{(*)}|}{\sqrt{2}|\mathcal{A}_{3/2}^{(*)}|}. \qquad (15)$$

In the HQET limit [36, 38], the factorization model predicts $\delta^{(*)} = 0$ and $R^{(*)} = 1$, while SCET [16, 17, 18] predicts δ to have the same value in the $D\pi$ and $D^*\pi$ systems. The strong phase $\delta^{(*)}$ can be computed with an isospin analysis of the $D^{(*)}\pi$ system. The input parameters are the world average values provided by the PDG 2007 partial update [24] of $\mathcal{BF}(B^- \to D^{(*)0}\pi^-)$, $\mathcal{BF}(\overline{B}^0 \to D^{(*)+}\pi^-)$ and of the B lifetime ratio $\tau(B^+)/\tau(B^0)$, the value of $\mathcal{BF}(\overline{B}^0 \to D^{(*)0}\pi^0)$ is the one measured in this analysis. We calculate the value of $\delta^{(*)}$ and $R^{(*)}$ using a frequentist

approach [37] $\delta = (30.2^{+3.2}_{-4.5})°$ and $R = 0.70^{+0.05}_{-0.05}$ for $D\pi$ final states, and $\delta^* = (13.6^{+9.9}_{-13.6})°$, $R^* = 0.64^{+0.06}_{-0.05}$ for $D^*\pi$ final states.

In both $D^*\pi$ and $D\pi$ cases, the amplitude ratio is significantly different from the factorization prediction $R^{(*)} = 1$. The strong phase is significantly different from zero in the system $D\pi$, which points out that non-factorizable FSI are not negligible. In the system $D^*\pi$ that phase δ^* is smaller and compatible with zero due to the lower value of the $\mathcal{BF}$ for $D^{*0}\pi^0$.

5.3   Comparison to theoretical predictions on $\mathcal{BF}$'s

Table 4 compares the $\mathcal{BF}$ measured with this analysis to the predictions by factorization [13, 2, 34, 35] and pQCD [14, 15]. We confirm the conclusion by the previous *BABAR* analysis, the values measured being higher by a factor of about 4 than the values predicted by factorization. The pQCD predictions are closer to experimental values but globally higher except for $D^0\pi^0$.

Table 4: Comparison of the measured branching fraction $\mathcal{BF}$ in units of 10^{-4}, with the predictions by factorization and pQCD [14, 15]. The first quoted uncertainty is statistical and the second is systematic.

$\overline{B}^0$ mode	This measurement ($\times 10^{-4}$)	factorization ($\times 10^{-4}$)	pQCD ($\times 10^{-4}$)
$D^0\pi^0$	$2.78 \pm 0.08 \pm 0.20$	0.58 [13] 0.70 [2]	2.3-2.6
$D^{*0}\pi^0$	$1.78 \pm 0.13 \pm 0.23$	0.65 [13] 1.00 [2]	2.7-2.9
$D^0\eta$	$2.41 \pm 0.09 \pm 0.17$	0.34 [13] 0.50 [2]	2.4-3.2
$D^{*0}\eta$	$2.32 \pm 0.13 \pm 0.22$	0.60 [2]	2.8-3.8
$D^0\omega$	$2.77 \pm 0.13 \pm 0.22$	0.66 [13] 0.70 [2]	5.0-5.6
$D^{*0}\omega$	$4.44 \pm 0.23 \pm 0.61$	1.70 [2]	4.9-5.8
$D^0\eta'$	$1.38 \pm 0.12 \pm 0.22$	0.30-0.32 [35]; 1.70-3.30 [34]	1.7-2.6
$D^{*0}\eta'$	$1.29 \pm 0.23 \pm 0.23$	0.41-0.47 [34]	2.0-3.2

Factorization predicts the ratio $\mathcal{BF}(\overline{B}^0 \to D^{(*)0}\eta')/\mathcal{BF}(\overline{B}^0 \to D^{(*)0}\eta)$ to have a value between 0.64 and 0.68 [34] linked to the $\eta - \eta'$ mixing. Table 5 compares that prediction with the experimental measurements. The measured ratios are smaller than the prediction and are compatible at $1\,\sigma$.

The effective theory SCET [16, 17, 18] does not predict the absolute value of the $\mathcal{BF}$ but that the ratios $\mathcal{BF}(\overline{B}^0 \to D^{*0}h^0)/\mathcal{BF}(\overline{B}^0 \to D^0h^0) \sim 1$ for $h^0 = \pi^0, \eta$ and η'. For $h^0 = \omega$ that prediction holds only for the longitudinal component of $\overline{B}^0 \to D^{*0}\omega$ as long-distance QCD interactions may increase the transverse amplitude. A measurement of f_L is therefor needed.

The SCET gives also a prediction about the ratio $\mathcal{BF}(\overline{B}^0 \to D^{(*)0}\eta')/\mathcal{BF}(\overline{B}^0 \to D^{(*)0}\eta) \simeq 0.67$, which is similar to the prediction by factorization.

The $\mathcal{BF}$ ratios are given in Table 5, the common systematics between D^0h^0 and $D^{*0}h^0$ are cancelled. The ratios $\mathcal{BF}(\overline{B}^0 \to D^{*0}h^0)/\mathcal{BF}(\overline{B}^0 \to D^0h^0)$ for $h^0 = \pi^0, \eta, \eta'$ are compatible with 1.

6   CONCLUSIONS

We measured the branching fractions of the color-suppressed decays $\overline{B}^0 \to D^{(*)0}h^0$, where $h^0 = \pi^0, \eta, \omega,$ and η' with $454 \times 10^6 B\overline{B}$ pairs. Our measurements are in agreement with the previous

Table 5: Ratios of branching fractions $\mathcal{BF}(\overline{B}^0 \to D^{*0}h^0)/\mathcal{BF}(\overline{B}^0 \to D^0h^0)$. The first uncertainty is statistical, the second is systematic.

$\mathcal{BF}$ ratio	This measurement
$\frac{\mathcal{BF}(D^{*0}\pi^0)}{\mathcal{BF}(D^0\pi^0)}$	$0.64 \pm 0.05 \pm 0.08$
$\frac{\mathcal{BF}(D^{*0}\eta(\gamma\gamma))}{\mathcal{BF}(D^0\eta(\gamma\gamma))}$	$1.01 \pm 0.08 \pm 0.08$
$\frac{\mathcal{BF}(D^{*0}\eta(\pi\pi\pi^0))}{\mathcal{BF}(D^0\eta(\pi\pi\pi^0))}$	$0.91 \pm 0.11 \pm 0.04$
$\frac{\mathcal{BF}(D^{*0}\eta)}{\mathcal{BF}(D^0\eta)}$	$0.96 \pm 0.06 \pm 0.07$
$\frac{\mathcal{BF}(D^{*0}\omega)}{\mathcal{BF}(D^0\omega)}$	$1.61 \pm 0.11 \pm 0.20$
$\frac{\mathcal{BF}(D^{*0}\eta'(\pi\pi\eta))}{\mathcal{BF}(D^0\eta'(\pi\pi\eta))}$	$0.87 \pm 0.22 \pm 0.04$
$\frac{\mathcal{BF}(D^{*0}\eta'(\rho^0\gamma))}{\mathcal{BF}(D^0\eta'(\rho^0\gamma))}$	$0.84 \pm 0.30 \pm 0.15$
$\frac{\mathcal{BF}(D^{*0}\eta')}{\mathcal{BF}(D^0\eta')}$	$0.93 \pm 0.19 \pm 0.11$
$\frac{\mathcal{BF}(D^0\eta')}{\mathcal{BF}(D^0\eta)}$	$0.57 \pm 0.06 \pm 0.06$
$\frac{\mathcal{BF}(D^{*0}\eta')}{\mathcal{BF}(D^{*0}\eta)}$	$0.55 \pm 0.11 \pm 0.04$

results [7, 9, 10] with a significant decrease of both statistical and systematic uncertainties. We confirm the significant difference from theoretical predictions by factorization quoted in the previous analysis [9] and provide strong constraints on the models of color-suppressed decays.

7   ACKNOWLEDGMENTS

References

[1] D. Du, Phys. Lett. B **406**, 110 (1997).

[2] M. Neubert and B. Stech, in *Heavy Flavours II*, eds. A.J. Buras and M. Lindner (World Scientific, Singapore, 1998), p. 294.

[3] M. Bauer, B. Stech and M. Wirbel, Z. Phys. C **34**, 103 (1987).

[4] M. Neubert and A.A. Petrov, Phys. Lett. B **519**, 50 (2001).

[5] A. Deandrea, N. Di Bartolomeo, R. Gatto, and G. Nardulli, Phys. Lett. B **318**, 549 (1993); A. Deandrea *et al.*, *ibid.* **320**, 170 (1994).

[6] K. Honscheid, K. R. Schubert, and R. Waldi, Z. Phys. C **63**, 117 (1994).

[7] CLEO Collaboration, T. E. Coan *et al.*, Phys. Rev. Lett. **88**, 062001 (2002).

[8] Belle Collaboration, K. Abe *et al.*, Phys. Rev. Lett. **88**, 052002 (2002).

[9] *BABAR* Collaboration, B. Aubert *et al.*, Phys. Rev. D **69**, 032004 (2004).

[10] Belle Collaboration, J. Schmann *et al.*, Phys. Rev. D **72**, 011103 (2005).

[11] Belle Collaboration, K. Abe *et al.*, Phys. Rev. D **74**, 092002 2006).

[12] Belle Collaboration, K. Abe *et al.*, (2007), Phys. Rev. D **76**, 012006 (2007).

[13] C-K. Chua, W-S. Hou, and K-C. Yang, Phys. Rev. D **65**, 096007 (2002).

[14] Y.Y Keum, T. Kurimoto, H. Li, C.D Lü and A.I. Sanda, Phys. Rev. D **69**, 094018 (2004).

[15] C.D Lü, Phys. Rev. D **68**, 097502 (2003).

[16] C. W. Bauer, D. Pirjol and I. W. Stewart, Phys. Rev. D **65**, 054022 (2002).

[17] A.E. Blechman, S. Mantry and I.W. Stewart, Phys. Lett. B **608**, 77 (2005).

[18] S. Mantry, D. Pirjol and I. W. Stewart, Phys. Rev. D **68** 114009 (2003), MIT-CTP-3370.

[19] *BABAR* Collaboration, B. Aubert *et al.*, Nucl. Instrum. Methods Phys. Res., Sect. A **479**, 1 (2002).

[20] D. Lange, Nucl. Instrum. Methods Phys. Res., Sect. A **462**, 152 (2001).

[21] T. Sjostrand, S. Mrenna and P. Skands, Comput. Phys. Commun. **178**, 852 (2008).

[22] T. Sjöstrand, Comput. Phys. Commun. **82**, 74 (1994).

[23] *GEANT*4 Collaboration, V. N. Ivanchenko *et al.*, Nucl. Instrum. Methods Phys. Res., Sect. A **494**, 514 (2002). *GEANT*4 Collaboration, S. Agostinelli *et al.*, *ibid.* **506**, 250 (2003).

[24] Particle Data Group, W.-M. Yao *et al.*, J. Phys. G 33, 1 (2006), and partial 2007 update for the 2008 edition.

[25] Collaboration E691, J.C. ANJOS *et al.*, Phys. Rev. D **48**, 56 (1993).

[26] A. Höcker *et al.*, TMVA Group, [arXiv:physics/0703039v4] (2007).

[27] *BABAR* note 870.

[28] *BABAR* note 87 and 867.

[29] The modified Novossibirsk function divides the fitting region in a peaking region, a low and a high tail regions. For a variable x, the modified Novosibirsk function $f(x)$ is:

in the peak region : $x_1 < x < x_2$,

$$f(x) = A_p \times \exp\left(-\ln(2)\left(\frac{\ln\left(1 + 2\tau\sqrt{\tau^2+1}\cdot\frac{x-x_p}{\sigma_p\sqrt{2\ln(2)}}\right)}{\ln(1+2\tau^2-2\tau\sqrt{\tau^2+1})}\right)^2\right), \tag{16}$$

in the low tail region: $x < x_1$,

$$f(x) = A_p \times \exp\left(\frac{\tau\sqrt{\tau^2+1}\cdot(x-x_1)\sqrt{2\ln(2)}}{\sigma_p(\sqrt{\tau^2+1}-\tau)^2\ln(\sqrt{\tau^2+1}+\tau)} + \rho_1\cdot\left(\frac{x-x_1}{x_p-x_1}\right)^2 - \ln 2\right). \tag{17}$$

in the high tail region: $x > x_2$,

$$f(x) = A_p \times \exp\left(-\frac{\tau\sqrt{\tau^2+1}\cdot(x-x_2)\sqrt{2\ln(2)}}{\sigma_p(\sqrt{\tau^2+1}+\tau)^2\ln(\sqrt{\tau^2+1}+\tau)} + \rho_2\cdot\left(\frac{x-x_2}{x_p-x_2}\right)^2 - \ln 2\right). \tag{18}$$

The parameters are:

- A_p is the value at the maximum of the function,
- x_p is the peak position,
- σ_p is the width of the peak defined as the width at half-height divided by 2.35.
- ξ is an asymmetry parameter.

The positions x_1 and x_2 are $x_{1,2} = x_p + \sigma_p\sqrt{2\ln 2}\cdot\left(\frac{\xi}{\sqrt{\xi^2+1}}\mp 1\right)$,

[30] CLEO Collaboration, G. Bonvicini *et al.*, CLEO CONF 98-23, ICHEP98 852, *Proceedings of XXVIV ICHEP, Vancouver, 1998.*

[31] CLEO Collaboration, S.E. Csorna *et al.*, Phys. Rev. D **67**, 112002 (2003).

[32] S.M. Berman, M. Jacob, Phys. Rev. Lett. **139**, 1023 (1965).

[33] J.L. Rosner, Phys. Rev. D **60**, 074028 (1999).

[34] A. Deandrea and A.D. Polosa, Eur. Phys. Jour. **22**, 677 (2002).

[35] J.O. Eeg, A. Hiorth and A.D. Polosa, Phys. Rev. D **65**, 054030 (2002).

[36] M. Beneke, G. Buchalla, M. Neubert and C. T. Sachradja, Nucl. Phys. B **591**, 313 (2000).

[37] CKMfitter Group (J. Charles et al.), Eur. Phys. Jour. C **41**, 1-131 (2005).

[38] H-Y. Cheng and K-C Yang, Phys. Rev. D **59**, 092004 (1999).